

Enhanced response of global wetland methane emissions to recent El Niño-Southern Oscillation events

Zhen Zhang^{1,2}, Niklaus E. Zimmermann^{2,3}, Leonardo Calle⁴, George Hurtt¹, Abhishek Chatterjee^{5,6}, Benjamin Poulter^{4,5}

¹Department of Geographical Sciences, University of Maryland, College Park, MD 20740, USA

²Dynamic Macroecology, Swiss Federal Research Institute WSL, Zürcherstrasse 111, Birmensdorf 8903, Switzerland

³Department of Environmental System Science, Swiss Federal Institute of Technology ETH, Zürich 8092, Switzerland

⁴Institute on Ecosystems and Department of Ecology, Montana State University, Bozeman, MT 59717, USA

⁵Biospheric Sciences Laboratory, NASA Goddard Space Flight Center, Greenbelt, MD 20771, USA

⁶Universities Space Research Association, Columbia, MD 21046, USA

Abstract: Wetlands are thought to be the major contributor to interannual variability in the growth rate of atmospheric methane (CH₄) with anomalies driven by the influence of the El Niño-Southern Oscillation (ENSO). However, it remains unclear whether the increase in total global CH₄ emissions during El Niño versus La Niña events is from wetlands and how large the contribution of wetland CH₄ emissions is to the interannual variability of atmospheric CH₄. Here, we use a terrestrial ecosystem model that includes permafrost and wetland dynamics to estimate CH₄ emissions, forced by three separate meteorological reanalyses and one gridded observational climate dataset, to simulate the spatio-temporal dynamics of wetland CH₄ emissions from 1980-2016. The results show that, although wetland CH₄ responds to El Niño events with negative anomalies during the El Niño periods, the instantaneous growth rate of wetland CH₄ emissions exhibits complex phase dynamics. All of our simulations suggest that a record-high wetland CH₄ growth rate was reached in the beginning of the 2015-2016 El Niño event. We also find evidence for a step increase of CH₄ emissions by 7.8 ± 1.6 Tg CH₄ yr⁻¹ during 2007-2014 compared to the average of 2000-2006 from simulations using meteorological reanalyses, which is equivalent to a ~ 3.5 ppb yr⁻¹ rise in CH₄ concentrations. The step increase is mainly caused by the expansion of wetland area in the tropics (30°S-30°N) due to an enhancement of tropical precipitation as indicated by the suite of the meteorological reanalyses. Our study highlights the role of wetlands in driving the variability and trends of atmospheric CH₄ concentrations and stresses the need to account for uncertainty in climate forcings in addressing the interannual variability and decadal-scale trends of wetland CH₄ fluxes.

Introduction

Methane (CH₄) is a potent greenhouse gas contributing to about 20% of the warming induced by long-lived greenhouse gases since pre-industrial times (IPCC, 2013). Atmospheric CH₄ concentrations have risen from preindustrial levels of 715 parts per billion (ppb) since the 1800s (Etheridge *et al.*, 1998; MacFarling Meure *et al.*, 2006) to current global concentration of ~1847 ppb, a 2.5-fold increase, primarily driven by anthropogenic activities (Kirschke *et al.*, 2013), e.g. fossil fuel activities, agriculture, and also by the biogeochemical feedbacks of natural processes to climate change (Arneeth *et al.*, 2010; Tian *et al.*, 2016; Saunio *et al.*, 2016). However, the variability in the annual growth rate of atmospheric CH₄ is considered to be strongly associated with the response of biogenic CH₄ sources to climate variability, in which global wetlands contributes 60-80% of biogenic emissions during the past (Quiquet *et al.*, 2015; Hopcroft *et al.*, 2017) and likely into the projected future (Zhang *et al.*, 2017b). Thus, the growth rate of atmospheric CH₄ is largely affected by the response of global wetland CH₄ emissions to the year-to-year mode of global climate variability like the El Niño-Southern Oscillation (ENSO), one of the largest climate phenomena that drives carbon fluxes and their anomalies across large portions of the globe (Chatterjee *et al.*, 2017).

El Niño, the positive phase of ENSO, influences the hydrologic and carbon cycle of tropical terrestrial ecosystems through a change in atmospheric pressure patterns and sea surface temperatures that induce strong warming and reduced precipitation patterns by shifting the Intertropical Convergence Zone southward, causing amplified wildfires (Worden *et al.*, 2013) and reduced wetland areal extent and CH₄ emissions (Hodson *et al.*, 2011). Tropical wetlands, which contribute 50-70% of the global wetland CH₄ emissions (Bousquet *et al.*, 2006), are largely affected by the periodic variations of air temperature and precipitation induced by ENSO phases (Pison *et al.*, 2013). However, in contrast to the findings from forward models, e.g. terrestrial biogeochemical models, which suggest that tropical and global wetland CH₄ emissions are usually found to decrease during El Niño (Hodson *et al.*, 2011; Zhu *et al.*, 2017; Ringeval *et al.*, 2014), atmospheric measurements show that the growth rate of global CH₄ concentration can rise during strong El Niño years (Nisbet *et al.*, 2016). In addition, the link between the annual CH₄ growth rate and the variability in global wetland CH₄ emissions has been challenged by the observed pause in the growth during 2000-2006, but following which, in 2007, a strong growth rate resumed (Nisbet *et al.*, 2014). Recent studies suggest that global wetlands played a limited role during the renewed rise through 2012 (Poulter *et al.*, 2017; Turner *et al.*, 2017; Rigby *et al.*, 2017). Meanwhile, isotopic measurements appear to indicate that the resumed increase in the growth rate rather originates from biogenic sources than from fossil-fuels (Schwietzke *et al.*, 2016), suggesting an increased influence of tropical wetlands (Nisbet *et al.*, 2016) or agricultural sources (Schaefer *et al.*, 2016). This calls for revisiting the role of teleconnections, and their timing, on wetlands and land-atmosphere CH₄ fluxes to help reconcile top-down and bottom-up methodologies.

Previous extreme El Niño events, in years 1982-1983, 1997-1998, and 2015-2016, had significant impacts on terrestrial ecosystems and are considered key drivers of the atmospheric CO₂ growth rate variability (Liu *et al.*, 2017). It has been reported that the latest El Niño event (2015-2016) was one of the strongest on record, causing unprecedented warming and extreme droughts over most of the Amazonia regions (Jiménez-Muñoz *et al.*, 2016; L'Heureux *et al.*, 2016; Lim *et al.*, 2017; Chatterjee *et al.*, 2017). The occurrence of this extreme El Niño event severely disrupted regional ecosystems, causing sharp increases in atmospheric CO₂ concentrations (Betts *et al.*, 2016) and a doubling of fire-induced emissions in Southeast Asia (Whitburn *et al.*, 2016). El Niño may have also contributed to record warming during 2015 and the first third of 2016, at 0.98°C above the 20th century mean monthly average (<http://www.ncdc.noaa.gov/sotc/global/201613>, last access at August 2017). Exactly how much the 2015-2016 ENSO phenomenon has impacted global wetland CH₄ emissions and to what extent it has affected the annual growth rate of atmospheric CH₄ concentration remains unknown due to challenges in monitoring and modeling.

Here, we analyze the relationship between ENSO phases and annual wetland CH₄ emissions by addressing two main questions. First, how does ENSO, with particular attention to the ENSO event in 2015-2016, affect the interannual variability of CH₄ emissions from global wetlands? Second, what is the relationship between the interannual variability of the growth in atmospheric CH₄ and wetland CH₄ emissions over the recent decade, and what are the major mechanisms linking wetland CH₄ emissions to the increases since 2007?

Methods

We use a process-based ecosystem model LPJ-wsl (Lund-Potsdam-Jena model, *WSL* version) forced with four different atmospheric forcings to simulate wetland CH₄ emissions from 1980 to 2016. The four climate products include one station-based monthly geo-interpolation dataset (CRU) and three meteorological reanalyses products. The reason for using multiple forcings is to investigate the uncertainty from meteorological forcings in driving the simulated atmospheric CH₄ concentrations, and hence to better characterizes the CH₄ variations in response to climate variability.

LPJ-wsl (Poulter *et al.*, 2011) is a process-based dynamic global vegetation model (DGVM) developed for studying terrestrial ecosystems, which is based on an earlier LPJ core model (Sitch *et al.*, 2003). The version of the model applied in this study includes a new hydrologic model TOPMODEL to determine wetland area and its inter- and intra-annual dynamics (Zhang *et al.*, 2016), a permafrost and dynamic snow model (Wania *et al.*, 2009), and a prognostic wetland CH₄ emission model (Hodson *et al.*, 2011), each of which is incorporated into the LPJ-wsl framework with consideration of the effects of snow and freeze/thaw cycles on CH₄ emissions

(Zhang *et al.*, 2016). The estimation of CH₄ emissions is based on an empirical model that considers soil respiration, inundated area, and a temperature-based ecosystem emission efficiency (Christensen *et al.*, 1996). The simulated variations in wetland areas and CH₄ emissions have been evaluated against large-scale observations in previous studies (Hodson *et al.*, 2011; Zhang *et al.*, 2016; Zhang *et al.*, 2017b). Here, we calibrated temperature-modified CH₄ emitting factors by scaling simulated global estimates to match 172 Tg CH₄ yr⁻¹ in 2004, which was estimated from an independent atmospheric inversion study (Spahni *et al.*, 2011), and in agreement with independent satellite-based methods from Bloom *et al.* (2010). We improved inundation estimates by calibrating the TOPMODEL parameter ‘maximum inundation potential’ (F_{\max}) (Zhang *et al.*, 2016) using an independent inundation dataset (Poulter *et al.*, 2017) that was derived from a satellite-based Surface Water Microwave Product Series (SWAMPS) (Schroeder *et al.*, 2015) and inventory-based dataset Global Lakes and Wetlands Database (GLWD) (Lehner and Döll, 2004), as well as from a regional wetland map derived from satellite retrievals for Amazonia (Hess *et al.*, 2015). To avoid confusion regarding double counting (Thornton *et al.*, 2016), we clarify that in this study simulated wetland area explicitly includes both permanently inundated vegetated wetlands and seasonally inundated wetlands, e.g. floodplains, but excludes reservoirs, large and small lakes and rivers, as well as coastal wetlands that are defined and constrained by GLWD, and rice agriculture.

The climate datasets included the monthly meteorology from the Climate Research Unit (CRU) TS 3.25 (Harris *et al.*, 2014), three state-of-the-art metrological reanalysis products, including 1-hourly reanalysis Modern-Era Retrospective analysis for Research and Applications Version 2 (MERRA2) (Gelaro *et al.*, 2017) from the NASA Global Modeling and Assimilation Office (GMAO), 6-hourly ERA-Interim (ERA-I) (Dee *et al.*, 2011) from the European Centre for Medium-Range Weather Forecasts (ECMWF) data assimilation system and 6-hourly Japanese 55-year Reanalysis (JRA-55) (Kobayashi *et al.*, 2015) from the Japan Meteorological Agency (JMA). To generate these three forcing datasets, four output products (total precipitation, 2m air temperature, downward shortwave radiation, and surface longwave radiation) were aggregated to a daily time-step and downscaled to a common 0.5° spatial resolution grid using bilinear interpolation to match the gridded soils input. For the monthly CRU data, LPJ-wsl was set up to use a wet-day frequency dataset, a weather generator (Geng *et al.*, 1986) to generate daily precipitations, and a set of simplified equations with monthly cloud cover as input to calculate mid-month daily photosynthetically active radiation flux and potential evapotranspiration (Prentice *et al.*, 1993). Additional details of the climate forcing datasets and model experiments are in Supplementary Material (Table S1). The LPJ-wsl state variables (i.e., carbon in vegetation, litter, and soils) were simulated to reach equilibrium by using a 1000-year spinup, with fire dynamics, and a 398-year spinup for land use change using Land-Use Harmonization dataset (LUHv2) (Hurt *et al.*). After equilibrium, a transient simulation with fire effects included was performed for the years 1901-2016 (for CRU) and 1980-2016 (for reanalysis), forced with changing climate conditions as prescribed. For the reanalysis

simulations, CO₂ concentrations were gradually increased starting from the spinup and recycling the meteorological information.

We used the Multivariate ENSO index (MEI) for representing the ENSO strength (Wolter and Timlin, 1998). The MEI index represents the first unrotated principal component of the combined, normalized fields of the primary climate variables observed over the tropical Pacific, reflecting a global signal of climate-land-atmosphere interaction for both El Niño and La Niña events; Given that studies on progressions of carbon fluxes during El Niño (Yuanyuan *et al.*, 2017; Liu *et al.*, 2017) have shown a hysteresis in the Earth system's response to changes in temperature and precipitation patterns, we carried out a cross-correlation analysis to examine possible time-lag effects of wetland CH₄ response to El Niño events.

To test whether annual wetland anomalies contributed to the growth rate of atmospheric CH₄, we compared our results against the annual mean global CH₄ growth rate and monthly CH₄ trend derived from NOAA/ESRL (Dlugokencky *et al.*, 1994). We then used the first derivative of spline-smoothed monthly wetland CH₄ anomalies as a metric for quantifying the growth rate of month wetland CH₄ emissions. The time series of CH₄ concentration measurements, derived from NOAA cooperative air sampling network, were processed with a curve fitting method (Thoning *et al.*, 1989) that decomposes the full signal into a long-term growth rate fit by a polynomial function, seasonal oscillations by a harmonic function and a low pass digital filter to retain interannual and short-term variations. From the decomposed signal, we derived the component signals such as trend, growth rate, and annual amplitude. The CH₄ amplitude of the seasonal cycle from Mauna Loa surface site (MLO: 19.53°N, 155.58°W) in NOAA/ESRL was applied to the analysis as a reflection of the strength of CH₄ seasonality, which is mainly controlled by CH₄ uptake and release processes of the land biosphere. Given that the wetlands contribute to the largest portion of natural CH₄ sources and the interannual variability of the major CH₄ sink, hydroxyl radical (OH) is relatively small (Montzka *et al.*, 2011), the changing trends in CH₄ amplitude consequently imply that they are largely affected by changing CH₄ dynamics in the wetland ecosystems. We compared the observed MLO CH₄ amplitude with simulated wetland CH₄ amplitude, which is calculated as the difference between maxima and minima in spline-smoothed monthly wetland CH₄ anomalies within one year, to test whether the simulated shifting patterns of wetland CH₄ dynamics is consistent with observations.

For evaluation of wetland areal changes we used terrestrial water storage (TWS) anomalies, observed by the Gravity Recovery and Climate Experiment (GRACE) satellite measurement, as a proxy for groundwater storage and surface inundation (Bloom *et al.*, 2012; Boening *et al.*, 2012). We used Level-3 monthly solutions from Geo Forschung Zentrum (GFZ), the University of Texas Center for Space Research (CSR), and the Jet Propulsion Laboratory (JPL) from April 2002 to December 2016 to analyze the time variations of the water mass changes in the tropics. The monthly TWS was multiplied by a spatial grid of scaling coefficients derived from post-processing of GRACE observations (Landerer and Swenson, 2012) to restore the

signals attenuated in the processing at small spatial scales. Given the ensemble mean was the most effective in reducing the noise in the gravity fields solutions (Sakumura *et al.*, 2014), we applied the ensemble mean of monthly TWS from three different products in the analysis.

Results and Discussion

Long-term response of wetland CH₄ to ENSO

The ensemble climate simulations indicate a strong link between ENSO and wetland CH₄ emissions, with higher emissions during La Niña and lower emissions during El Niño (Figure 1a). We find a significant negative correlation (d.f. = 443, $p < 0.01$) between the ENSO MEI index and monthly wetland CH₄ anomalies, regardless of the climate data used in the simulations. This is consistent with the findings from bottom-up modeling estimates (Hodson *et al.*, 2011; McNorton *et al.*, 2016; Zhu *et al.*, 2017), atmospheric modeling (Pison *et al.*, 2013; Chen and Prinn, 2006) and satellite observations. For example, the atmospheric CH₄ observations from the Infrared Atmospheric Sounding Interferometer (IASI) aboard METOP and the Atmospheric Infrared Sounder (AIRS) aboard NASA's Aqua satellite also suggest similar findings in that column-averaged dry-air mole fractions of CH₄ (XCH₄) show higher increase in 2007-2008 and 2010-2011 when strong La Niña events occurred (Xiong *et al.*, 2016). Airborne-based estimates of the interannual variability of CH₄ fluxes for eastern Amazon Basin also provides ancillary evidence that the CH₄ emissions are greatest in 2008, a year of La Niña phase (Basso *et al.*, 2016). Recent satellite observations from the Greenhouse gases Observing SATellite (GOSAT) also suggest large-scale fluctuations in atmospheric CH₄ during ENSO events, indicating that wetland CH₄ emissions are ~5% higher during La Niña events (Pandey *et al.*, 2017). The increase in CH₄ emissions from wetlands during La Niña can be attributed predominantly to a large increase in flood extents, primarily over tropical areas (including SE Australia, northern South America, and Southeast Asia) (Boening *et al.*, 2012), whereas the decreases during El Niño are possibly due to drought-induced shrinking of flooded areas. All of the evidence above suggests a robust negative relationship between anomalies of wetland CH₄ emissions and ENSO events, i.e., positive anomalies during La Niña and vice versa.

However, negative anomalies of wetland CH₄ emissions do not necessarily lead to a decrease in the growth rate of wetland CH₄ emissions during El Niño. We find that the growth rate of wetland CH₄ emissions is in a rising phase during strong El Niño events with the amplitudes of the growth rate varied, with the strength dependent on which meteorological forcing was used in the simulations (Figure 1b). This is mainly because strong El Niño events exhibit negative CH₄ growth rates at the beginning of the ENSO anomaly, but then the growth rate rapidly recovers to positive values. Despite that the largely decreased inundations caused declines in CH₄ emissions at the beginning of strong El Niño phases, the extremely high temperatures over the tropics strongly increase the CH₄ growth rate due to higher

soil decomposition rates. Cross-correlation analyses between the monthly growth rate of wetland CH₄ emissions and the MEI index suggest that the peak correlation occurs at a 3-month lag (when ENSO leads $\Delta\text{CH}_4/\Delta t$) for the globe. As expected, the timing of wetland response to ENSO varies regionally, where Tropical Asia and Tropical South America exhibit a ~4 month lag and no lag, respectively (Figure S1). The IAV of wetland CH₄ emissions is dominated by the Tropics (30°S-30°N) with relatively small contributions from the Northern Hemisphere (Figures 1c, 1d). MERRA2 showed the highest IAV among all four simulations, whereas the CRU-based simulation had the lowest IAV. The rise of wetland CH₄ emission growth rate is consistent with the observed spikes of atmospheric CH₄ growth rates during strong El Niño events (Dlugokencky *et al.*, 1998).

Impact of 2015-2016 El Niño on wetland CH₄

Annual growth in CH₄ emissions from global wetlands during the 2015-2016 El Niño surpassed any growth rate previously observed, including the growth rate observed during two strong El Niño events, in 1982-1983 and 1997-1998. Our simulations captured the magnitude of this large increase in wetland CH₄ emissions with an instantaneous growth rate of $\sim 7.6 \pm 1.6$ Tg CH₄ yr⁻¹ during 2015-2016 El Niño. The meteorological datasets drove instantaneous growth rates that ranged between 9.2 Tg CH₄ month⁻¹, 8.6 Tg CH₄ yr⁻¹, 7.2 Tg CH₄ yr⁻¹, and 5.5 Tg CH₄ yr⁻¹ using MERRA2, JRA-55, CRU, and ERA-I, respectively. Although the 2015-2016 El Niño was not as strong as the 1997-1998 El Niño according to the MEI index (~ 3 in 1997-1998 and ~ 2.5 in 2015-2016), the combined effect of rising CO₂ concentrations and high temperatures most likely amplified the impact, causing 1.8 times the maximum growth rate of CH₄ of the 1997-1998 El Niño event (mean growth rate of $\sim 4.2 \pm 1.4$ Tg CH₄ yr⁻¹ for the respective time period).

The spatial distribution of wetland CH₄ anomalies demonstrated that the large increases in soil respiration drove the strong growth rate and occurred during the March-April-May (MAM) season in 2016 as a consequence of warming and droughts in this summer (October 2015 - May 2016) (Figure 2). There was a widespread increase in CH₄ emissions over western Amazonia, mainly attributed to increased soil respiration resulting from drought-induced mortality. Despite a large decline in wetland extent due to severe drought, significant positive anomalies in CH₄ emission peaked across the western Amazonian basin, likely due to high temperatures. A number of studies reported that hot and dry conditions during El Niño caused tree mortality and declines in biomass growth and resulted in increased litter and carbon release (Jones and Cox, 2005; Keeling *et al.*, 1995), which is consistent with LPJ-wsl simulated results. Temperature is the primary climatic variable driving the long-term trend and resulting increase in CH₄ emissions (Zhang *et al.*, 2017b). However, precipitation is the dominant climatic variable regulating interannual variability in CH₄ emissions by altering the inundation extent and creating anaerobic conditions suitable for methanogenesis in the tropics (Zhang *et al.*, 2017b). In addition, the higher CO₂ concentrations in 2016 compared to levels during the 1997-1998 El Niño have enhanced the impact of temperature on CH₄ IAV through a

positive feedback on primary production from CO₂ fertilization effects. This has led to increased soil carbon substrate availability for microbial decomposition and a positive feedback is therefore modeled in LPJ-wsl and in most of the land surface models (Wania *et al.*, 2013).

Wetland CH₄ trends between 2000-2006 and post-2007

Using the meteorological reanalysis data, we find evidence for a step increase in global annual wetland emissions between the periods of 2007-2014 relative to that of 2000-2006 (Figure 3a). These simulations suggest that the average annual CH₄ emissions from 2007-2014 increased by $\sim 7.8 \pm 1.6$ Tg CH₄ yr⁻¹ compared to the average of 2000-2006, which is equivalent to an increase in the growth rate of up to ~ 3.5 ppb CH₄ yr⁻¹ for the post-2007 period, or about half of the observed increase in concentrations. Interestingly, CRU-based simulation in this study did not show a strong step-increase between these two periods, suggesting an insignificant contribution only from wetlands with a 1.5 Tg CH₄ yr⁻¹ increase in the post-2007 resume of the growth rate. This is consistent with the findings from an ensemble modeling experiment using CRU as forcing dataset, which did not result in a significant increase of global wetland CH₄ emissions to the period of renewed atmospheric CH₄ growth (Poulter *et al.*, 2017). Another recent atmospheric modeling study, also using CRU as forcing for their prior inputs, suggested likewise that wetlands made only a small contribution to the post-2007 growth with ~ 1 ppb/yr (McNorton *et al.*, 2016). In contrast, all our simulations using meteorological reanalysis data suggest that more than 90% of the increase in the growth rate of wetland CH₄ is from the Tropics (Table 2), mainly due to increases in precipitation across the South America, Tropical Africa, and Southeast Asia since 2007. MERRA2-based simulations suggest that the post-2007 rise in global CH₄ concentrations primarily comes from South America and Tropical Africa, whereas ERA-I and JRA-55 identify South America as the largest contributor to the CH₄ growth rate (Figure S2).

The different IAV patterns of CH₄ emissions among these simulations suggest that the uncertainties in climate drivers in estimation of CH₄ emissions (Figure 3a). The model experiments demonstrated that the discrepancy is mainly from different model behavior when using products like CRU and meteorological reanalyses like MERRA2, ERA-I, and JRA-55, regardless of the temporal resolution of climate inputs used (Figure S3). We found only minor differences between using daily and monthly temporal resolution, which likely reduced uncertainties from applying the weather generator and thus show that the weather generator covered the internal climatic variability at monthly scale. The importance of considering uncertainty of climate forcing was also reflected in the representation of the seasonal cycle of CH₄ emissions. The comparison of simulated CH₄ emissions with independent estimates using an atmospheric model STILT based on CARVE airborne experiments (Zona *et al.*, 2016) suggested a dominant role of climate forcings in capturing CH₄ seasonality in arctic regions (Figure 3b). MERRA2, ERA-Interim, and JRA-55 underestimated the peak CH₄ emission in growing season but were able to capture the general seasonal

cycle in CH₄ emissions for the North Slope of Alaska, while CRU-based estimates failed to reproduce a similar pattern. The seasonal cycle of CH₄ emissions was also generally underestimated by most bottom-up models that used CRU climate data in a synthesis modeling experiment (Melton *et al.*, 2013), highlighting the need to better constrain the CH₄ emissions by taking into account several datasets that represent climate forcing uncertainty.

Sensitivity of wetland CH₄ emissions to ENSO

To further investigate whether the influence of ENSO on global wetland CH₄ fluctuation was strengthening, we evaluated the average sensitivity of simulated wetland CH₄ emissions and wetland areas in the tropics to ENSO events by calculating the ratio of the annual anomaly of CH₄ emission/wetland area to the annual MEI index for three different time periods, 1980-1999, 2000-2006, and 2007-2016 (Figure 4). We observed a minor change in the sensitivity of CH₄ emissions and wetland areas between 1980-1999 and 2000-2006, which suggest a dampened feedback of global wetland CH₄ emissions to increasing global temperatures. However, the sensitivity became enhancing post-2007. The sensitivity of the modeled results was strongly increased for the period of 2007-2016 relative to the two previous time periods. The sensitivity in CH₄ emissions was increased by ~200% in MERRA2, ERA-I, and JRA-55, whereas the CRU run resulted in a lower percent increase (42%) compared to the other model experiments. The concurrent increase in the sensitivity of CH₄ emissions and wetland areas indicates that the increase of CH₄ emissions since 2007 can mainly be attributed to an increased sensitivity of wetland areas, which was driven by the changing precipitation patterns found in meteorological reanalysis products. The GRACE measurement for relative equivalent water storage confirms the large increase for the period of 2007-2014 compared to earlier periods (Figure 5), suggesting that our simulated increases in tropical wetland areas are robust. All of the modeled wetland areas have significant correlations (d.f.=176, p <0.01) with GRACE TWS, and suggest a ~0.15 Mkm² increase in inundation over time period of 2007-2014. This also implies that, despite an observed decline in open water in the tropics (due to the anthropogenic effect from denser population and impact of human activities for the period of 1990s and early 2000s (Prigent *et al.*, 2012)), an increase in precipitation since 2007 was primarily related to La Niña induced precipitation anomalies over Australia, Southeast Asia, and northern South America, which possibly affected wetland patterns and CH₄ emissions globally.

Relationship between wetland CH₄ and atmospheric growth rate

There was a statistically significant (90%-level) positive trend in the simulated annual amplitude of wetland CH₄ emissions, suggesting an increasingly enhanced sensitivity of wetland CH₄ emissions to climate change in recent decades (Figure 6). All model simulations indicated positive trends of the annual amplitude of wetland CH₄ emissions with small differences depending on climate forcings. These simulated positive trends are consistent with observed trends in CH₄ amplitude at

the MLO site, for which MERRA2, ERA-I, and JRA-55 runs were well correlated with MLO observations (d.f. = 30, $p < 0.05$) and only CRU-based simulations showed a weak correlation between wetland CH₄ emissions and enhanced global CH₄ seasonality. These significant correlations suggest that the seasonal amplitude of atmospheric CH₄ concentrations are largely driven by the seasonal cycle of natural wetland emissions. The increasing trends in CH₄ amplitude also imply a high likelihood that there is an underlying shift of CH₄ seasonality in wetland ecosystems and this shift in seasonality is likely greatest in tropical regions.

We found a small, but significant, positive correlation between annual wetland CH₄ emissions and the annual atmospheric CH₄ growth rate in simulations forced by the daily meteorological datasets MERRA2 ($R = 0.31$, d.f. = 33, $p < 0.1$), ERA ($R = 0.36$, d.f. = 33, $p < 0.1$), and JRA-55 ($R = 0.38$, d.f. = 33, $p < 0.05$) for the period of 2000-2015, whereas no significant correlation was found in CRU-based runs ($R = 0.07$, d.f. = 33, $p > 0.75$). For the period of 1980-1999, none of the simulations showed a significant correlation with the annual atmospheric CH₄ growth rate. The atmospheric CH₄ growth rate is not exclusively a result of changes in wetland emissions, but rather due to a combined influence of anthropogenic and natural sources, and also due to a hydroxyl radical sink (Turner *et al.*, 2017; Rigby *et al.*, 2017). Combined with recent studies reporting the estimated increase in annual CH₄ emissions from global livestock (Wolf *et al.*, 2017) and observed expansion of agricultural areas for rice paddies in Southern Asia (Zhang *et al.*, 2017a), where precipitation has largely increased since 2007, we hypothesize that a combination of tropical wetlands and agricultural sources have most strongly contributed to the resumption in growth rate of atmospheric CH₄ concentrations, which is consistent with the depletion in isotopic signature ¹³CH₄ (Schaefer *et al.*, 2016).

Conclusions

We demonstrate that global wetland CH₄ emission anomalies are strongly related to ENSO variability using an extended, multi-meteorological ensemble. At sub-annual time-scales, we also found that the instantaneous growth rate of wetland CH₄ anomalies was positively correlated with ENSO strengths, which provides an explanation for the observed rise of atmospheric CH₄ growth rate during strong El Niño events. The ongoing warming trend, as well as the shifting patterns of global precipitation, has likely had a significant impact on increasing global CH₄ interannual variability. The strong El Niño event in 2015-2016, associated with extreme heat and drought over the Amazonian regions, caused record-high growth rates of wetland CH₄ emissions compared to the previous three decades. We also found an increasing wetland sensitivity to ENSO oscillation since 2007, which we attribute to increased precipitations in the tropics as is visible from three meteorological reanalysis datasets, MERRA2, ERA-Interim, and JRA-55. Our study highlights the need to accurately account for uncertainties in the climate forcing in CH₄ estimations.

Acknowledgements

This study is funded in part by the Gordon and Betty Moore Foundation through Grant GBMF5439 “Quantifying Sources and Sinks in the Global Methane Cycle” to Zhen Zhang, George Hurtt, and Benjamin Poulter. We thank the Competence Center Environment and Sustainability (CCES) project Modeling and Experiments on Land-Surface Interactions with Atmospheric Chemistry and Climate Phase 2 (MAIOLICA2) #42-01, and the National Natural Science Foundation of China (T411391009) for additional funding. We further thank NASA for preparing the MERRA2 dataset, the European Centre for Medium-Range Weather Forecasts for preparing the ERA-Interim dataset, the Japan Meteorological Agency for preparing the Japanese 55-year Reanalysis (JRA-55) dataset, and the Climate Research Unit at the University of East Anglia for providing the CRU dataset. We finally thank the NOAA ESRL Global Monitoring Division for providing CH₄ measurements. We thank Sara H. Knox for constructive comments on the manuscript.

Data availability

The global wetland areal dynamics and CH₄ emissions in this study are available upon request from the corresponding author. Atmospheric CH₄ concentration datasets were obtained from the NOAA ESRL GMD Carbon Cycle Cooperative Global Air Sampling Network (<https://www.esrl.noaa.gov/gmd/ccgg/flask.php>, last access at August 2017). The annual mean global CH₄ growth rate and monthly trend were derived from NOAA/ESRL (www.esrl.noaa.gov/gmd/ccgg/trends_ch4/). Terrestrial Water Storage products were derived from the GRACE website (<https://grace.jpl.nasa.gov/data/get-data/>, last accessed on October 2017). We used the multivariate ENSO index (MEI) (<https://www.esrl.noaa.gov/psd/enso/mei/>) as indices for representing ENSO strength.

References:

- Arneth A, Harrison S P, Zaehle S, Tsigaridis K, Menon S, Bartlein P J, Feichter J, Korhola A, Kulmala M, O'Donnell D, Schurgers G, Sorvari S and Vesala T 2010 Terrestrial biogeochemical feedbacks in the climate system *Nature Geosci* **3** 525-32
- Basso L S, Gatti L V, Gloor M, Miller J B, Domingues L G, Correia C S C and Borges V F 2016 Seasonality and interannual variability of CH₄ fluxes from the eastern Amazon Basin inferred from atmospheric mole fraction profiles *Journal of Geophysical Research. Atmospheres* **121** 168-84
- Betts R A, Jones C D, Knight J R, Keeling R F and Kennedy J J 2016 El Niño and a record CO₂ rise *Nature Clim. Change* **6** 806-10
- Bloom A A, Palmer P I, Fraser A and Reay D S 2012 Seasonal variability of tropical wetland CH₄ emissions: the role of the methanogen-available carbon pool *Biogeosciences* **9** 2821-30
- Bloom A A, Palmer P I, Fraser A, Reay D S and Frankenberg C 2010 Large-Scale Controls of Methanogenesis Inferred from Methane and Gravity Spaceborne Data *Science* **327** 322-5
- Boening C, Willis J K, Landerer F W, Nerem R S and Fasullo J 2012 The 2011 La Niña: So strong, the oceans fell *Geophysical Research Letters* **39** n/a-n/a
- Bousquet P, Ciais P, Miller J B, Dlugokencky E J, Hauglustaine D A, Prigent C, Van der Werf G R, Peylin P, Brunke E G, Carouge C, Langenfelds R L, Lathiere J, Papa F, Ramonet M, Schmidt M, Steele L P, Tyler S C and White J 2006 Contribution of anthropogenic and natural sources to atmospheric methane variability *Nature* **443** 439-43
- Chatterjee A, Gierach M M, Sutton A J, Feely R A, Crisp D, Eldering A, Gunson M R, O'Dell C W, Stephens B B and Schimel D S 2017 Influence of El Niño on atmospheric CO₂ over the tropical Pacific Ocean: Findings from NASA's OCO-2 mission *Science* **358**
- Chen Y-H and Prinn R G 2006 Estimation of atmospheric methane emissions between 1996 and 2001 using a three-dimensional global chemical transport model *Journal of Geophysical Research: Atmospheres* **111** 2156-202
- Christensen T R, Prentice I C, Kaplan J, Haxeltine A and Sitch S 1996 Methane flux from northern wetlands and tundra *Tellus B* **48** 652-61
- Dee D P, Uppala S M, Simmons A J, Berrisford P, Poli P, Kobayashi S, Andrae U, Balmaseda M A, Balsamo G, Bauer P, Bechtold P, Beljaars A C M, van de Berg L, Bidlot J, Bormann N, Delsol C, Dragani R, Fuentes M, Geer A J, Haimberger L, Healy S B, Hersbach H, Hólm E V, Isaksen I, Kållberg P, Köhler M, Matricardi M, McNally A P, Monge-Sanz B M, Morcrette J J, Park B K, Peubey C, de Rosnay P, Tavolato C, Thépaut J N and Vitart F 2011 The ERA-Interim reanalysis: configuration and performance of the data assimilation system *Quarterly Journal of the Royal Meteorological Society* **137** 553-97
- Dlugokencky E J, Masarie K A, Lang P M and Tans P P 1998 Continuing decline in the growth rate of the atmospheric methane burden *Nature* **393** 447

- Dlugokencky E J, Steele L P, Lang P M and Masarie K A 1994 The growth rate and distribution of atmospheric methane *Journal of Geophysical Research: Atmospheres* **99** 17021-43
- Etheridge D M, Steele L P, Francey R J and Langenfelds R L 1998 Atmospheric methane between 1000 A.D. and present: Evidence of anthropogenic emissions and climatic variability *Journal of Geophysical Research: Atmospheres* **103** 15979-93
- Gelaro R, McCarty W, Suárez M J, Todling R, Molod A, Takacs L, Randles C A, Darmenov A, Bosilovich M G, Reichle R, Wargan K, Coy L, Cullather R, Draper C, Akella S, Buchard V, Conaty A, Silva A M d, Gu W, Kim G-K, Koster R, Lucchesi R, Merkova D, Nielsen J E, Partyka G, Pawson S, Putman W, Rienecker M, Schubert S D, Sienkiewicz M and Zhao B 2017 The Modern-Era Retrospective Analysis for Research and Applications, Version 2 (MERRA-2) *Journal of Climate* **30** 5419-54
- Geng S, Penning de Vries F W T and Supit I 1986 A simple method for generating daily rainfall data *Agricultural and Forest Meteorology* **36** 363-76
- Harris I, Jones P D, Osborn T J and Lister D H 2014 Updated high-resolution grids of monthly climatic observations – the CRU TS3.10 Dataset *International Journal of Climatology* **34** 623-42
- Hodson E L, Poulter B, Zimmermann N E, Prigent C and Kaplan J O 2011 The El Niño–Southern Oscillation and wetland methane interannual variability *Geophysical Research Letters* **38** L08810
- Hopcroft P O, Valdes P J, O'Connor F M, Kaplan J O and Beerling D J 2017 Understanding the glacial methane cycle *Nature Communications* **8** 14383
- Hurt G, Chini L, Sahajpal R and Frohling S Harmonization of global land-use change and management for the period 850-2100 *Geoscientific Model Development (In prep)*.
- IPCC 2013 *Climate Change 2013: The Physical Science Basis. Contribution of Working Group I to the Fifth Assessment Report of the Intergovernmental Panel on Climate Change* (Cambridge, United Kingdom and New York, NY, USA: Cambridge University Press)
- Jiménez-Muñoz J C, Mattar C, Barichivich J, Santamaría-Artigas A, Takahashi K, Malhi Y, Sobrino J A and Schrier G v d 2016 Record-breaking warming and extreme drought in the Amazon rainforest during the course of El Niño 2015–2016 *Scientific Reports* **6** 33130
- Jones C D and Cox P M 2005 On the significance of atmospheric CO₂ growth rate anomalies in 2002–2003 *Geophysical Research Letters* **32** n/a-n/a
- Keeling C D, Whorf T P, Wahlen M and van der Plicht J 1995 Interannual extremes in the rate of rise of atmospheric carbon dioxide since 1980 *Nature* **375** 666-70
- Kirschke S, Bousquet P, Ciais P, Saunoy M, Canadell J G, Dlugokencky E J, Bergamaschi P, Bergmann D, Blake D R, Bruhwiler L, Cameron-Smith P, Castaldi S, Chevallier F, Feng L, Fraser A, Heimann M, Hodson E L, Houweling S, Josse B, Fraser P J, Krummel P B, Lamarque J-F, Langenfelds R L, Le Quere C, Naik V, O'Doherty S, Palmer P I, Pison I, Plummer D, Poulter B, Prinn R G, Rigby M, Ringeval B, Santini M, Schmidt M, Shindell D T, Simpson I J, Spahni

- R, Steele L P, Strode S A, Sudo K, Szopa S, van der Werf G R, Voulgarakis A, van Weele M, Weiss R F, Williams J E and Zeng G 2013 Three decades of global methane sources and sinks *Nature Geosci* **6** 813-23
- Kobayashi S, Ota Y, Harada Y, Ebata A, Moriya M, Onoda H, Onogi K, Kamahori H, Kobayashi C, Endo H, Miyaoka K and Takahashi K 2015 The JRA-55 Reanalysis: General Specifications and Basic Characteristics *Journal of the Meteorological Society of Japan. Ser. II* **93** 5-48
- L'Heureux M L, Takahashi K, Watkins A B, Barnston A G, Becker E J, Di Liberto T E, Gamble F, Gottschalck J, Halpert M S, Huang B, Mosquera-Vásquez K and Wittenberg A T 2016 Observing and Predicting the 2015/16 El Niño *Bulletin of the American Meteorological Society* **98** 1363-82
- Landerer F W and Swenson S C 2012 Accuracy of scaled GRACE terrestrial water storage estimates *Water Resources Research* **48** n/a-n/a
- Lehner B and Döll P 2004 Development and validation of a global database of lakes, reservoirs and wetlands *Journal of Hydrology* **296** 1-22
- Lim Y-K, Kovach R M, Pawson S and Vernieres G 2017 The 2015/16 El Niño Event in Context of the MERRA-2 Reanalysis: A Comparison of the Tropical Pacific with 1982/83 and 1997/98 *Journal of Climate* **30** 4819-42
- Liu J, Bowman K W, Schimel D S, Parazoo N C, Jiang Z, Lee M, Bloom A A, Wunch D, Frankenberg C, Sun Y, O'Dell C W, Gurney K R, Menemenlis D, Gierach M, Crisp D and Eldering A 2017 Contrasting carbon cycle responses of the tropical continents to the 2015–2016 El Niño *Science* **358**
- MacFarling Meure C, Etheridge D, Trudinger C, Steele P, Langenfelds R, van Ommen T, Smith A and Elkins J 2006 Law Dome CO₂, CH₄ and N₂O ice core records extended to 2000 years BP *Geophysical Research Letters* **33** n/a-n/a
- McNorton J, Gloor E, Wilson C, Hayman G D, Gedney N, Comyn-Platt E, Marthews T, Parker R J, Boesch H and Chipperfield M P 2016 Role of regional wetland emissions in atmospheric methane variability *Geophysical Research Letters* n/a-n/a
- Melton J R, Wania R, Hodson E L, Poulter B, Ringeval B, Spahni R, Bohn T, Avis C A, Beerling D J, Chen G, Eliseev A V, Denisov S N, Hopcroft P O, Lettenmaier D P, Riley W J, Singarayer J S, Subin Z M, Tian H, Zürcher S, Brovkin V, van Bodegom P M, Kleinen T, Yu Z C and Kaplan J O 2013 Present state of global wetland extent and wetland methane modelling: conclusions from a model inter-comparison project (WETCHIMP) *Biogeosciences* **10** 753-88
- Montzka S A, Krol M, Dlugokencky E, Hall B, Jöckel P and Lelieveld J 2011 Small Interannual Variability of Global Atmospheric Hydroxyl *Science* **331** 67-9
- Nisbet E G, Dlugokencky E J and Bousquet P 2014 Methane on the Rise—Again *Science* **343** 493-5
- Nisbet E G, Dlugokencky E J, Manning M R, Lowry D, Fisher R E, France J L, Michel S E, Miller J B, White J W C, Vaughn B, Bousquet P, Pyle J A, Warwick N J, Cain M, Brownlow R, Zazzeri G, Lanoisellé M, Manning A C, Gloor E, Worthy D E J, Brunke E G, Labuschagne C, Wolff E W and Ganesan A L 2016 Rising atmospheric methane: 2007–2014 growth and isotopic shift *Global Biogeochemical Cycles* **30** 1356-70

- Pandey S, Houweling S, Krol M, Aben I, Monteil G, Nechita-Banda N, Dlugokencky E J, Detmers R, Hasekamp O, Xu X, Riley W J, Poulter B, Zhang Z, McDonald K C, White J W C, Bousquet P and Röckmann T 2017 Enhanced methane emissions from tropical wetlands during the 2011 La Niña *Scientific Reports* **7** 45759
- Pison I, Ringeval B, Bousquet P, Prigent C and Papa F 2013 Stable atmospheric methane in the 2000s: key-role of emissions from natural wetlands *Atmos. Chem. Phys.* **13** 11609-23
- Poulter B, Bousquet P, Canadell G J, Ciais P, Peregón A, Saunio M, Arora K V, Beerling J D, Brovkin V, Jones D C, Joos F, Gedney N, Ito A, Kleinen T, Koven D C, McDonald K, Melton R J, Peng C, Peng S, Prigent C, Schroeder R, Riley J W, Saito M, Spahni R, Tian H, Taylor L, Viovy N, Wilton D, Wiltshire A, Xu X, Zhang B, Zhang Z and Zhu Q 2017 Global wetland contribution to 2000–2012 atmospheric methane growth rate dynamics *Environmental Research Letters* **12** 094013
- Poulter B, Frank D C, Hodson E L and Zimmermann N E 2011 Impacts of land cover and climate data selection on understanding terrestrial carbon dynamics and the CO₂ airborne fraction *Biogeosciences* **8** 2027-36
- Prentice I C, Martin T S and Wolfgang C 1993 A simulation model for the transient effects of climate change on forest landscapes *Ecological Modelling* **65** 51-70
- Prigent C, Papa F, Aires F, Jimenez C, Rossow W B and Matthews E 2012 Changes in land surface water dynamics since the 1990s and relation to population pressure *Geophysical Research Letters* **39** L08403
- Quiquet A, Archibald A T, Friend A D, Chappellaz J, Levine J G, Stone E J, Telford P J and Pyle J A 2015 The relative importance of methane sources and sinks over the Last Interglacial period and into the last glaciation *Quaternary Science Reviews* **112** 1-16
- Rigby M, Montzka S A, Prinn R G, White J W C, Young D, O'Doherty S, Lunt M F, Ganesan A L, Manning A J, Simmonds P G, Salameh P K, Harth C M, Mühle J, Weiss R F, Fraser P J, Steele L P, Krummel P B, McCulloch A and Park S 2017 Role of atmospheric oxidation in recent methane growth *Proceedings of the National Academy of Sciences* **114** 5373-7
- Ringeval B, Houweling S, van Bodegom P M, Spahni R, van Beek R, Joos F and Röckmann T 2014 Methane emissions from floodplains in the Amazon Basin: challenges in developing a process-based model for global applications *Biogeosciences* **11** 1519-58
- Sakumura C, Bettadpur S and Bruinsma S 2014 Ensemble prediction and intercomparison analysis of GRACE time-variable gravity field models *Geophysical Research Letters* **41** 1389-97
- Saunio M, Jackson R B, Bousquet P, Poulter B and Canadell J G 2016 The growing role of methane in anthropogenic climate change *Environmental Research Letters* **11** 120207
- Schaefer H, Fletcher S E M, Veidt C, Lassey K R, Brailsford G W, Bromley T M, Dlugokencky E J, Michel S E, Miller J B, Levin I, Lowe D C, Martin R J, Vaughn B H and White J W C 2016 A 21st century shift from fossil-fuel to biogenic methane emissions indicated by 13CH₄ *Science* **352** 80-4

- Schroeder R, McDonald K, Chapman B, Jensen K, Podest E, Tessler Z, Bohn T and Zimmermann R 2015 Development and Evaluation of a Multi-Year Fractional Surface Water Data Set Derived from Active/Passive Microwave Remote Sensing Data *Remote Sensing* **7** 15843
- Schwietzke S, Sherwood O A, Bruhwiler L M P, Miller J B, Etiope G, Dlugokencky E J, Michel S E, Arling V A, Vaughn B H, White J W C and Tans P P 2016 Upward revision of global fossil fuel methane emissions based on isotope database *Nature* **538** 88-91
- Sitch S, Smith B, Prentice I C, Arneth A, Bondeau A, Cramer W, Kaplan J O, Levis S, Lucht W, Sykes M T, Thonicke K and Venevsky S 2003 Evaluation of ecosystem dynamics, plant geography and terrestrial carbon cycling in the LPJ dynamic global vegetation model *Global Change Biology* **9** 161-85
- Thoning K W, Tans P P and Komhyr W D 1989 Atmospheric carbon dioxide at Mauna Loa Observatory: 2. Analysis of the NOAA GMCC data, 1974-1985 *Journal of Geophysical Research: Atmospheres* **94** 8549-65
- Thornton B F, Wik M and Crill P M 2016 Double counting challenges the accuracy of high latitude methane inventories *Geophysical Research Letters* n/a-n/a
- Tian H, Lu C, Ciais P, Michalak A M, Canadell J G, Saikawa E, Huntzinger D N, Gurney K R, Sitch S, Zhang B, Yang J, Bousquet P, Bruhwiler L, Chen G, Dlugokencky E, Friedlingstein P, Melillo J, Pan S, Poulter B, Prinn R, Saunois M, Schwalm C R and Wofsy S C 2016 The terrestrial biosphere as a net source of greenhouse gases to the atmosphere *Nature* **531** 225-8
- Turner A J, Frankenberg C, Wennberg P O and Jacob D J 2017 Ambiguity in the causes for decadal trends in atmospheric methane and hydroxyl *Proceedings of the National Academy of Sciences* **114** 5367-72
- Wania R, Melton J R, Hodson E L, Poulter B, Ringeval B, Spahni R, Bohn T, Avis C A, Chen G, Eliseev A V, Hopcroft P O, Riley W J, Subin Z M, Tian H, van Bodegom P M, Kleinen T, Yu Z C, Singarayer J S, Zürcher S, Lettenmaier D P, Beerling D J, Denisov S N, Prigent C, Papa F and Kaplan J O 2013 Present state of global wetland extent and wetland methane modelling: methodology of a model inter-comparison project (WETCHIMP) *Geosci. Model Dev.* **6** 617-41
- Whitburn S, Van Damme M, Clarisse L, Turquety S, Clerbaux C and Coheur P F 2016 Doubling of annual ammonia emissions from the peat fires in Indonesia during the 2015 El Niño *Geophysical Research Letters* **43** 11,007-11,14
- Wolf J, Asrar G R and West T O 2017 Revised methane emissions factors and spatially distributed annual carbon fluxes for global livestock *Carbon Balance and Management* **12** 16
- Wolter K and Timlin M S 1998 Measuring the strength of ENSO events: How does 1997/98 rank? *Weather* **53** 315-24
- Worden J, Wecht K, Frankenberg C, Alvarado M, Bowman K, Kort E, Kulawik S, Lee M, Payne V and Worden H 2013 CH₄ and CO distributions over tropical fires during October 2006 as observed by the Aura TES satellite instrument and modeled by GEOS-Chem *Atmos. Chem. Phys.* **13** 3679-92
- Xiong X, Han Y, Liu Q and Weng F 2016 Comparison of Atmospheric Methane Retrievals From AIRS and IASI *IEEE Journal of Selected Topics in Applied Earth Observations and Remote Sensing* **9** 3297-303

- Yuanyuan F, Anna M M, Christopher R S, Deborah N H, Joseph A B, Philippe C, Shilong P, Benjamin P, Joshua B F, Robert B C, Daniel H, Maoyi H, Akihiko I, Atul J, Huimin L, Chaoqun L, Jiafu M, Nicholas C P, Shushi P, Daniel M R, Xiaoying S, Bo T, Hanqin T, Weile W, Yaxing W and Jia Y 2017 Global land carbon sink response to temperature and precipitation varies with ENSO phase *Environmental Research Letters* **12** 064007
- Zhang G, Xiao X, Biradar C M, Dong J, Qin Y, Menarguez M A, Zhou Y, Zhang Y, Jin C, Wang J, Doughty R B, Ding M and Moore Iii B 2017a Spatiotemporal patterns of paddy rice croplands in China and India from 2000 to 2015 *Science of The Total Environment* **579** 82-92
- Zhang Z, Zimmermann N E, Kaplan J O and Poulter B 2016 Modeling spatiotemporal dynamics of global wetlands: comprehensive evaluation of a new sub-grid TOPMODEL parameterization and uncertainties *Biogeosciences* **13** 1387-408
- Zhang Z, Zimmermann N E, Stenke A, Li X, Hodson E L, Zhu G, Huang C and Poulter B 2017b Emerging role of wetland methane emissions in driving 21st century climate change *Proceedings of the National Academy of Sciences* **114** 9647-52
- Zhu Q, Peng C, Ciais P, Jiang H, Liu J, Bousquet P, Li S, Chang J, Fang X, Zhou X, Chen H, Liu S, Lin G, Gong P, Wang M, Wang H, Xiang W and Chen J 2017 Interannual variation in methane emissions from tropical wetlands triggered by repeated El Niño Southern Oscillation *Global Change Biology* n/a-n/a
- Zona D, Gioli B, Commane R, Lindaas J, Wofsy S C, Miller C E, Dinardo S J, Dengel S, Sweeney C, Karion A, Chang R Y-W, Henderson J M, Murphy P C, Goodrich J P, Moreaux V, Liljedahl A, Watts J D, Kimball J S, Lipson D A and Oechel W C 2016 Cold season emissions dominate the Arctic tundra methane budget *Proceedings of the National Academy of Sciences* **113** 40-5

Figures:

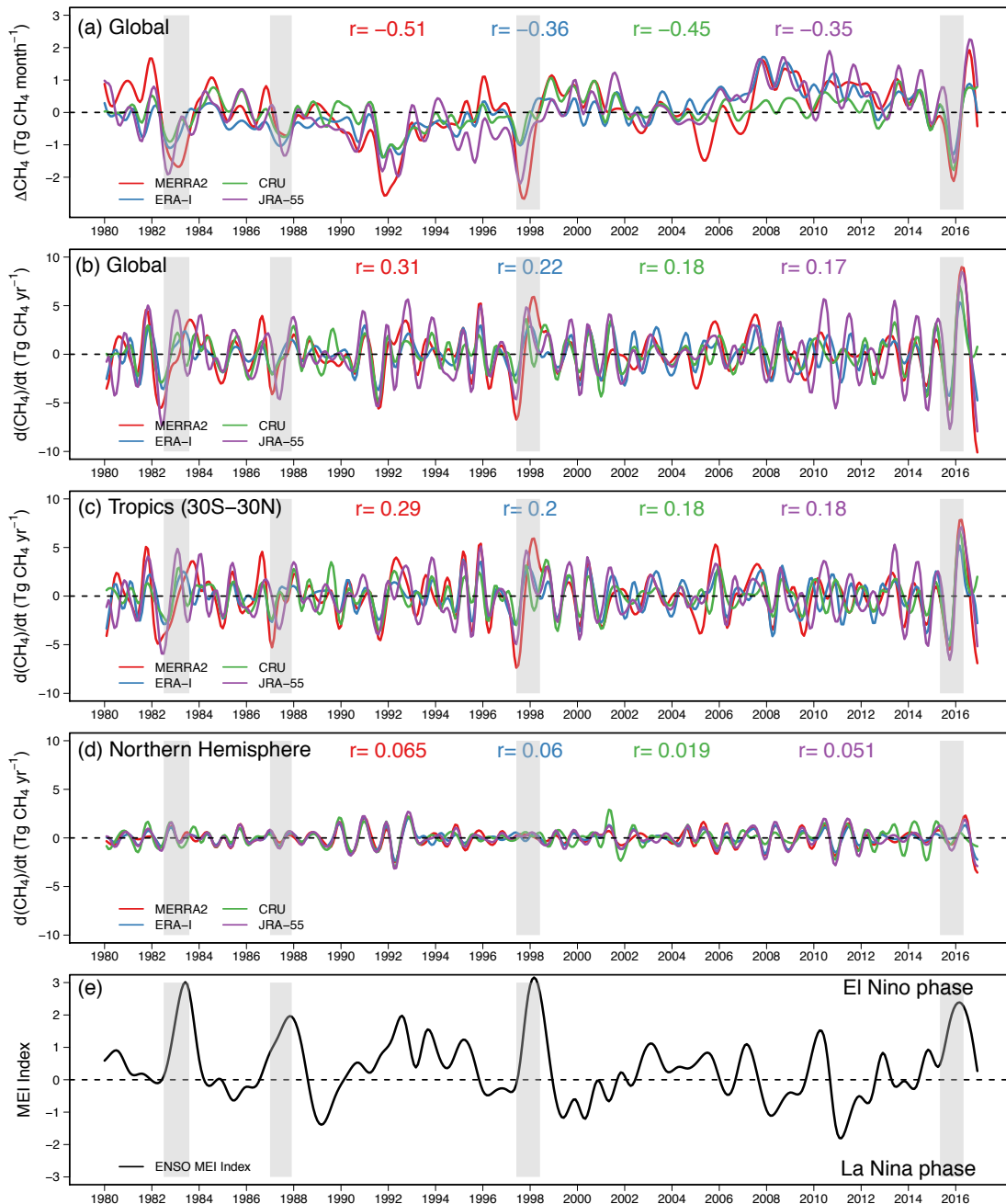


Figure 1. Global anomalies of monthly wetland CH_4 emissions (a) and instantaneous growth rates of wetland CH_4 emission anomalies from 1980 to 2016 for the Global (b), Tropics (middle, 30°S - 30°N) (c), and Northern Hemisphere (bottom, $>30^\circ\text{N}$) (d). The global anomalies of wetland CH_4 emissions were calculated relative to monthly average from 1980-2016. The instantaneous growth rate for each simulation is a time derivative of the smoothed monthly CH_4 anomalies using spline functions. The Spearman rank correlation coefficients between the multivariate ENSO index (MEI) and monthly wetland anomalies were derived from cross correlation analyses

(Figure S1) at 3 month lags (Lag= -3), with different colors corresponding to specific runs. Shaded grey areas represent the strong El Niño phases with MEI strength > 60 according to MEI ranks (<https://www.esrl.noaa.gov/psd/enso/mei/rank.html>, last access at January 2018).

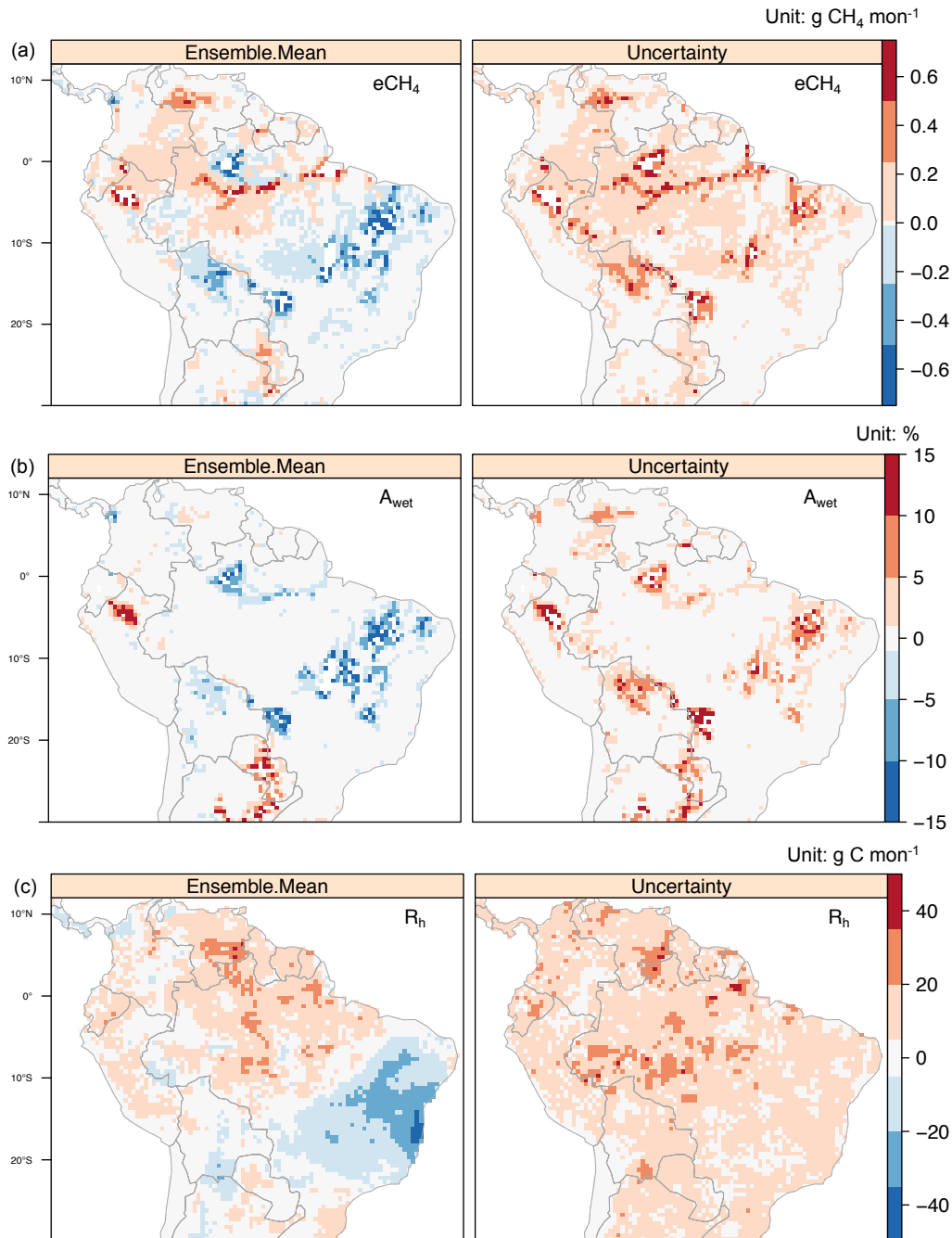


Figure 2. Spatial distributions of seasonal ensemble mean anomalies in wetland CH_4 emissions (a: $e\text{CH}_4$, Unit: $\text{g CH}_4 \text{ m}^{-2} \text{ mon}^{-1}$), inundated areas (b: A_{wet} , Unit: %), and heterotrophic respiration (c: R_h , Unit: $\text{g C m}^{-2} \text{ mon}^{-1}$) of the greater Amazonia region for the March-April-May season, 2016, where $e\text{CH}_4$ shows the highest growth rate during the 2015-2016 ENSO event. The anomalies are calculated as seasonal means during the MAM season of 2016 relative to average over the period of 1980-2016 level, with the uncertainty calculated as one-standard deviation from the four simulations forced by each meteorological dataset.

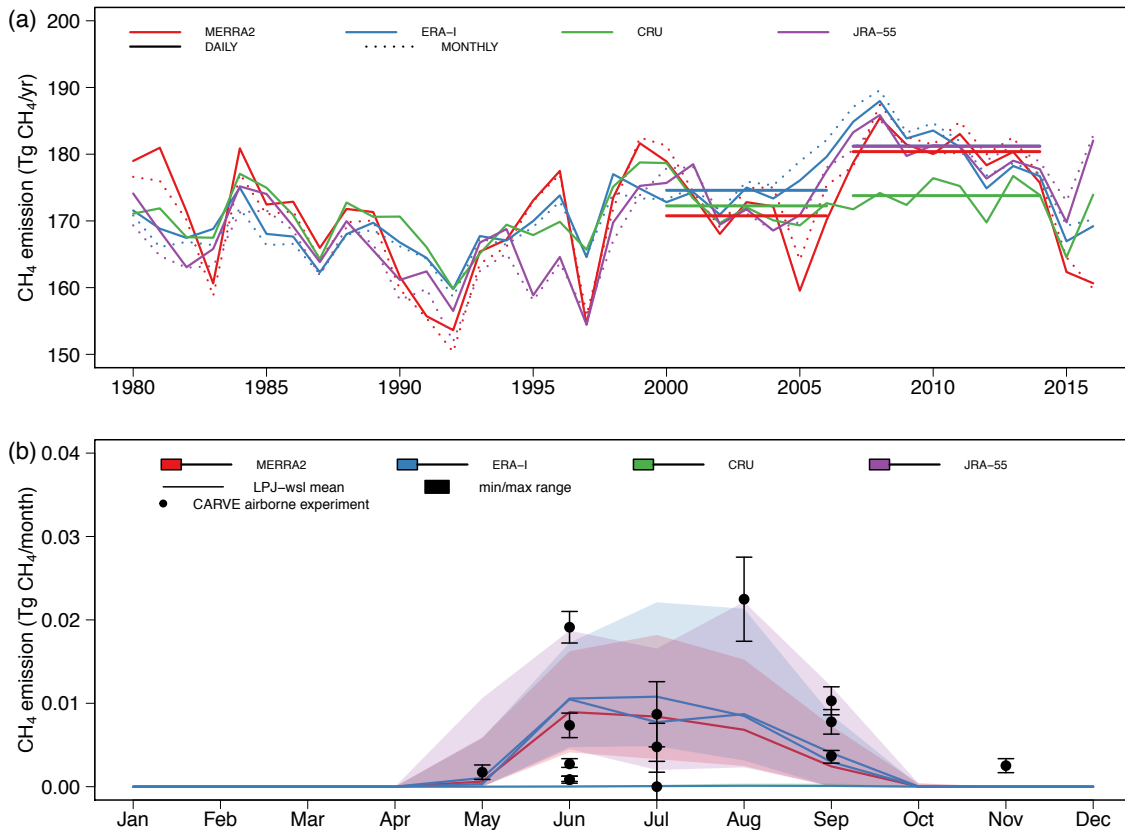


Figure 3. Simulated temporal patterns of CH₄ from all model experiments (see details in Table 1). (a) Time series of annual CH₄ emissions using climate forcings with daily and monthly temporal resolution. The daily forcings were aggregated to monthly values to evaluate the influence of daily variations of climate variables on CH₄ estimations. Solid and dotted lines represent daily and monthly inputs, respectively. The horizontal lines represent averaged annual CH₄ emissions for two time periods, 2000-2006 and 2007-2014, with the different colors representing different climate forcings. (b) Seasonal cycle between LPJ-wsl simulated monthly CH₄ fluxes (black line) using different climate forcings, with min/maximum range (areal shaded) over the Northern Slope of Alaska for 2012-2014 in comparison to the observed regional CH₄ fluxes (dots) estimated from analysis of 15 aircraft flights by the National Aeronautics and Space Administration's Carbon in Arctic Vulnerability Experiment (CARVE).

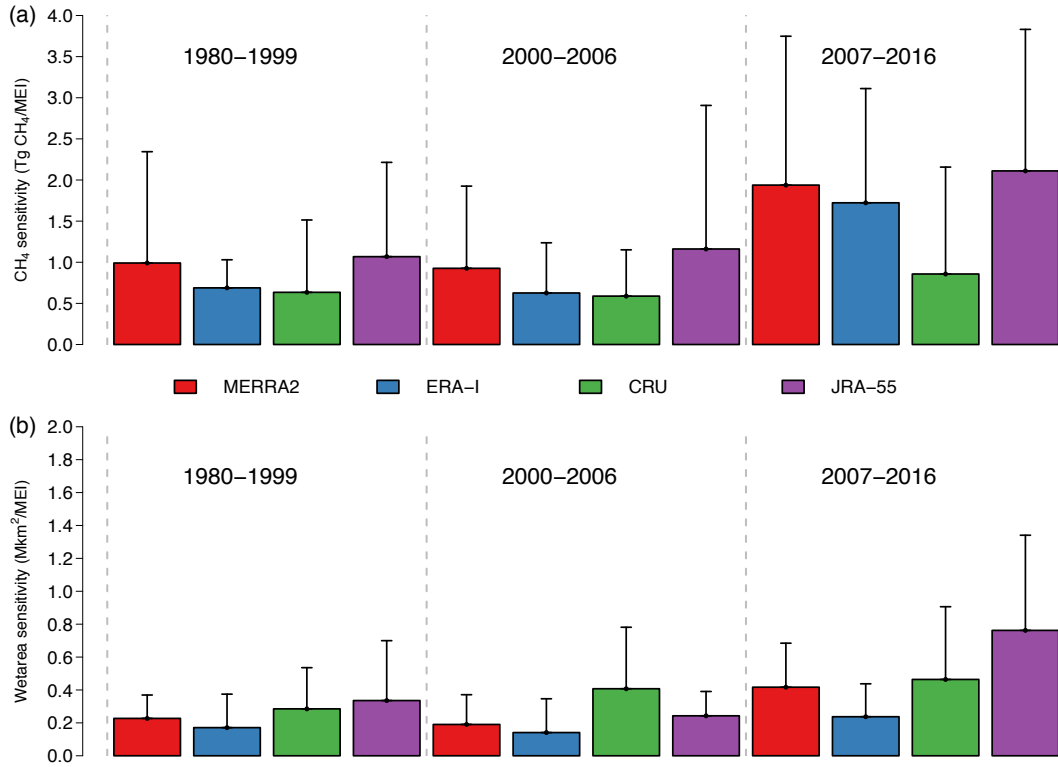


Figure 4. Sensitivity of (a) wetland CH₄ anomalies (Unit: Tg CH₄ /yr/MEI) and (b) wetland area anomalies for the tropics (Unit: Mkm²/yr/MEI; Mkm² = 10⁶ km²) to global ENSO strength for the period of 1980-1999, 2000-2006, and 2007-2016. The sensitivity metric is calculated as the ratio of averaged annual cumulative anomalies of wetland CH₄ emissions and wetland areas to the MEI index. Bars represent the modeled sensitivity from experiments with different forcing datasets, and the error bars represent one standard deviation.

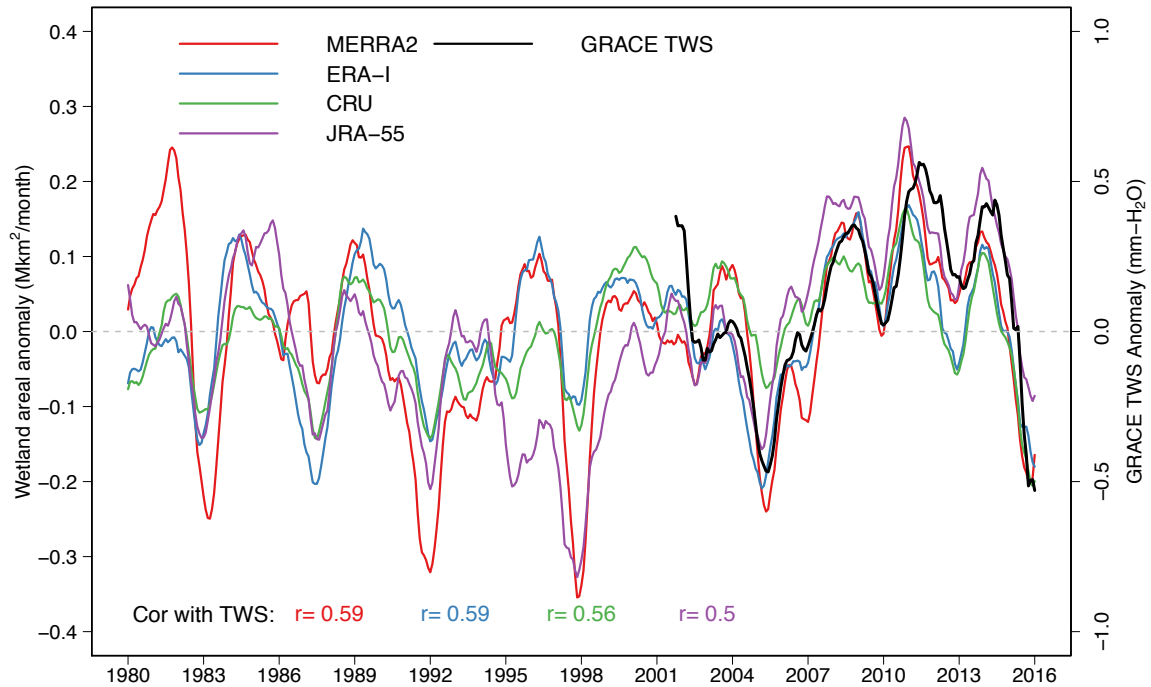


Figure 5. Trends of simulated wetland areal anomalies (Unit: Mkm²/month; Mkm²=10⁶ km²) for the tropics (30°S-30°N) compared to area-weighted average terrestrial water storage (TWS; Unit: mm-H₂O) from the ensemble mean of GRACE satellite measurement. The wetland anomalies were calculated relative to the monthly mean of 1980-2016, while TWS anomalies were relative to means of the 2004-2009 period. The fitted trends were calculated by smoothing the monthly anomalies with a 12-month moving average. The Spearman rank correlation coefficients between model and TWS are given for each simulation with different climate forcings in corresponding colors.

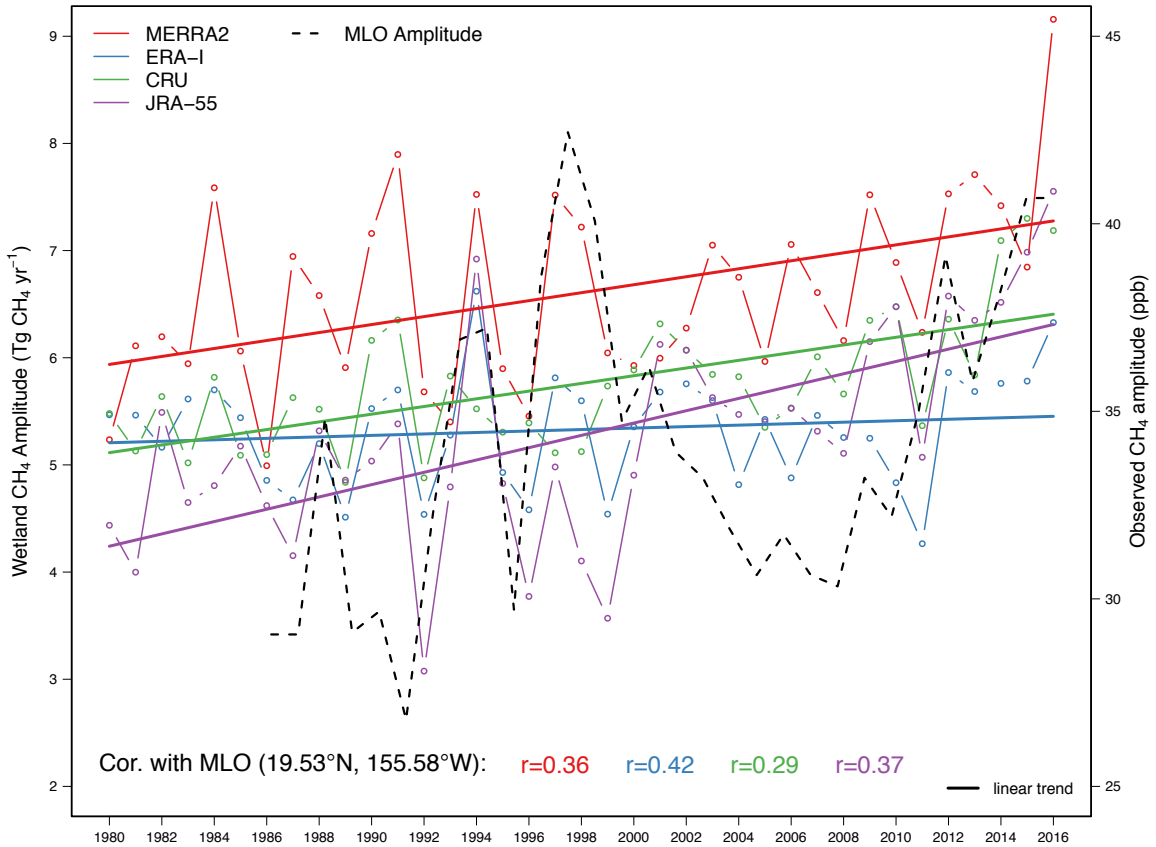


Figure 6. Time series of the seasonal amplitudes of global CH₄ fluxes. The seasonal amplitude of CH₄ fluxes (dashed dotted line) is calculated as the difference between maxima and minima of simulated monthly CH₄ emissions. The dashed black line represents observed peak-to-through seasonal amplitude of atmospheric CH₄ concentration at Mauna Loa observational station. The solid lines represent linear fitted long-term trends of the seasonal CH₄ cycle with Spearman rank correlation coefficients between models and observed amplitudes listed for each model runs in corresponding colors.

Tables:

Table 1. Model experiment descriptions. Climatic variables T, P, SW, LW, CLD, and WETD represent temperature, precipitation, shortwave radiation, longwave radiation, cloud cover, and wet days respectively.

Run ID number	Forcing	Temporal Resolution	Climatic Variables	Time periods
i	MERRA2	Daily	T, P, SW, LW	1980-2016
ii	MERRA2	Monthly	T, P, SW, LW*	1980-2016
iii	ERA-Interim	Daily	T, P, SW, LW	1980-2016
iv	ERA-Interim	Monthly	T, P, SW, LW	1980-2016
v	JRA-55	Daily	T, P, SW, LW	1980-2016
vi	JRA-55	Monthly	T, P, SW, LW*	1980-2016
vii	CRU	Monthly	T, P, CLD, WETD	1901-2016

*CLD and WETD are from CRU for comparison

Table 2. Summary of mean annual CH₄ emissions of the Tropics (30°S-30°N, denoted as TRO), the Northern Extratropics (denoted as NET), and the Southern Extratropics (denoted SET) for 2000-2006, and 2007-2014 from simulations with daily meteorological forcings MERRA2, ERA-I, and JRA-55 and with a spatial-interpolated climate dataset CRU that is based on interpolations from meteorological stations.

Time period	Forcing	eCH ₄ (Tg CH ₄ yr ⁻¹)			
		TRO	NET	SET	Global
2000-2006	CRU	138.1	32.3	1.8	172.2
	MERRA2	136.1	32.5	2.1	170.7
	ERA-Interim	142.3	26.6	1.9	170.9
	JRA-55	141.5	29.8	1.8	173.1
2007-2014	CRU	139.1	33.0	1.7	173.8
	MERRA2	145.6	32.8	1.9	180.3
	ERA-Interim	148.6	27.0	1.8	177.4
	JRA-55	147.7	31.1	1.8	180.6

Supplementary Information:

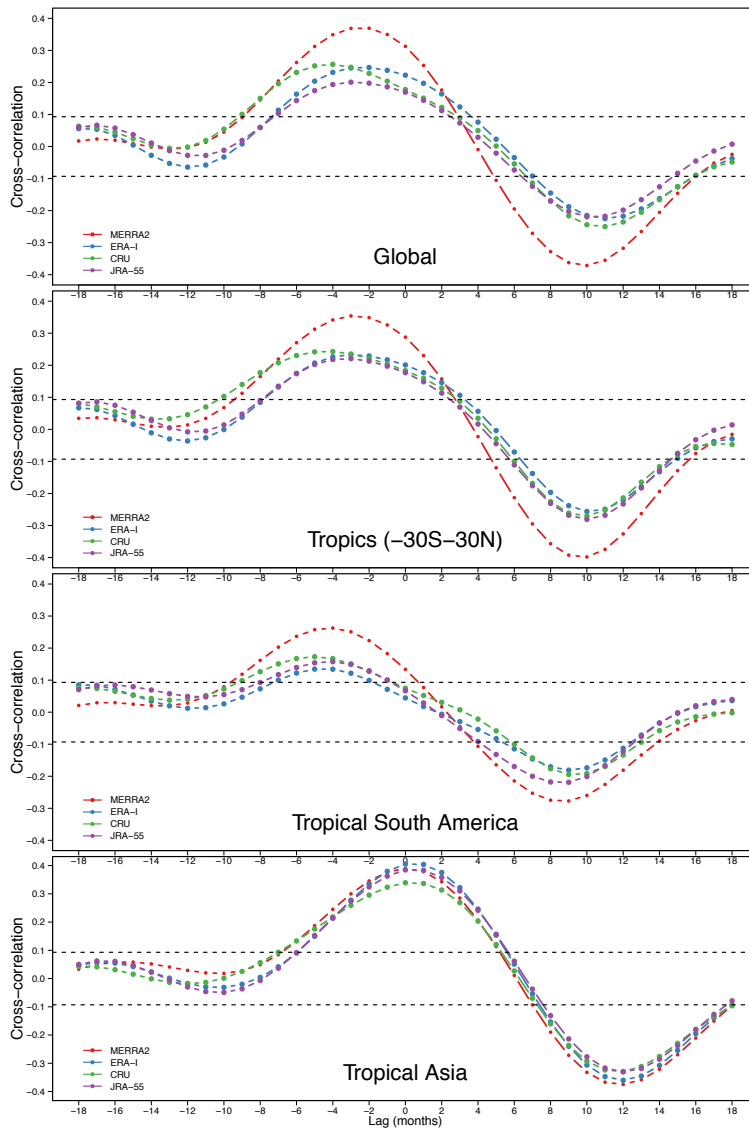


Figure S1. Cross-correlation analysis between ENSO MEI index and instantaneous growth rate of wetland CH₄ anomalies (calculated as time derivative of deseasonalized monthly wetland CH₄ emissions) from four simulations with different forcings (MERRA2, ERA-I, CRU, JRA-55). Dashed horizontal blue lines in all panels represent the 95% confidence interval.

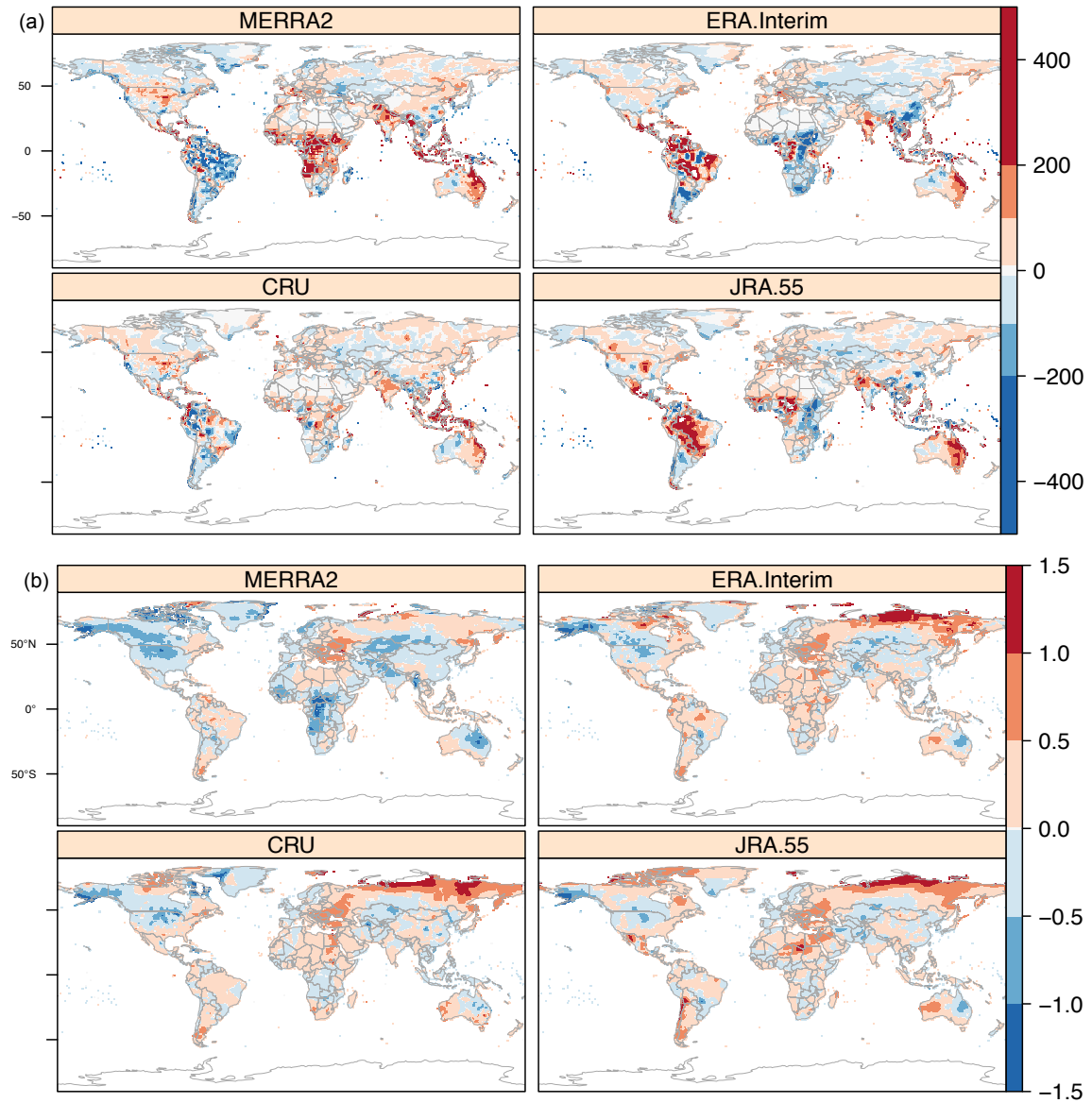


Figure S2. Spatial distribution of the mean difference in (a) precipitation (Unit: mm yr⁻¹) and (b) temperature (Unit: °C yr⁻¹) between 2007-2014 and 2000-2006 for MERRA2 and ERA-Interim.

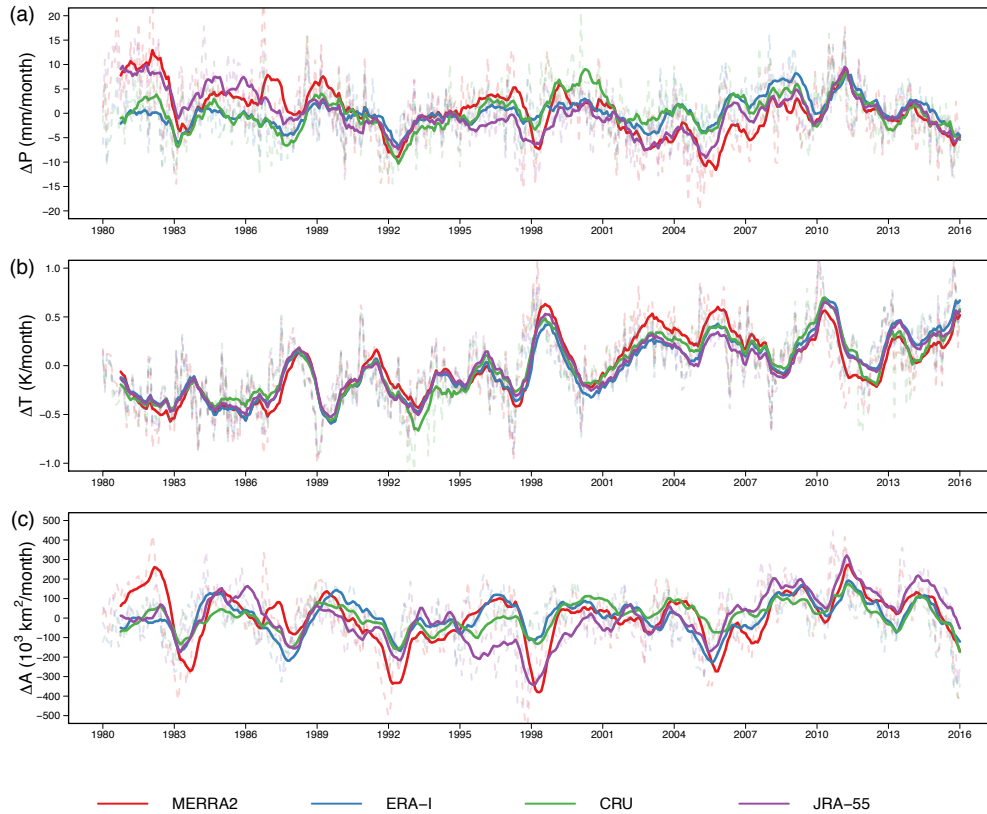


Figure S3. Time series of climate variables and simulated wetland area for the monthly anomalies of (a) precipitation (ΔP), (b) temperature (ΔT), and (c) wetland area (ΔA) in the tropics (30°S - 30°N). Monthly anomalies were estimated relative to corresponding long-term monthly mean (1980-2016). Dashed and solid lines represent the monthly anomaly and 12-month moving average respectively.